Lithos 320–321 (2018) 93–104

Contents lists available at ScienceDirect

Lithos

journal homepage: www.elsevier.com/locate/lithos

In-situ Sr-Pb isotope geochemistry of lawsonite: A new method to investigate slab-fluids

Tomomi Hara [a,*], Tatsuki Tsujimori [a,b], Qing Chang [c], Jun-Ichi Kimura [c]

[a] Department of Earth Science, Graduate School of Science, Tohoku University, Aoba, Sendai 980-8578, Japan
[b] Center for Northeast Asian Studies, Tohoku University, Aoba, Sendai 980-8576, Japan
[c] Department of Solid Earth Geochemistry, Japan Agency for Marine-Earth Science and Technology (JAMSTEC), Yokosuka 237-0061, Japan

ARTICLE INFO

Article history:
Received 2 April 2018
28 August 2018
Accepted 1 September 2018
Available online 6 September 2018

Keywords:
Lawsonite
Sr-Pb isotope
Trace element
Subduction zone fluid
South Motagua Mélange

ABSTRACT

Lawsonite is a hydrous Ca-Al silicate mineral which is broadly stable under modern style subduction conditions. In order to understand the elemental fractionation and the sources of subducted materials, lawsonite crystals in lawsonite-eclogite facies basaltic and sedimentary rocks from South Motagua Mélange of Guatemala were investigated using LA-ICPMS and LA-MC-ICPMS. Mass balance calculation based on *in-situ* trace element and modal compositions in an eclogite with a low-variance mineral assemblage confirmed that lawsonite hosts most of the light rare earth element (LREE), Sr, Pb, Th and U in the bulk. *In-situ* Sr-Pb isotope analyses of eclogite-facies lawsonite crystals revealed isotopic variations reflecting their protoliths. Isotopic zoning was also detected in some crystals. Lawsonite crystals in a phengite-rich eclogite have relatively low $^{87}Sr/^{86}Sr = 0.70335–0.70355$ with variations in $^{207}Pb/^{206}Pb = 0.8401–0.8512$ and $^{208}Pb/^{206}Pb = 2.0757–2.0911$. Lawsonite crystals from another eclogite are remarkably zoned. The cores have $^{87}Sr/^{86}Sr = 0.70558–0.70601$ and the rims have relatively elevated $^{87}Sr/^{86}Sr = 0.70636–0.70662$, exhibiting MORB-like $^{207}Pb/^{206}Pb = 0.843–0.844$ at the cores and more enriched $^{207}Pb/^{206}Pb = 0.839–0.841$ at the rims. The radiogenic Sr isotope composition would have been derived from seafloor alteration before subduction. In fact, lawsonite crystals in a metachert have higher $^{87}Sr/^{86}Sr = 0.70697–0.70757$ with $^{208}Pb/^{206}Pb = \sim 2.07$. However, the isotopically zoned metabasaltic lawsonite crystals with MORB-like core compositions suggest that metasomatism by an external fluid from sediment protolith occurred during overgrowth of their rims. Our study indicates that lawsonite crystals record both the isotopic compositions of the protoliths and metasomatic fluids from different protoliths. The *in-situ* Sr-Pb isotope analysis has a potential to reveal records of the complicated metamorphic processes.

1. Introduction

Since the onset of plate tectonics, convergent plate margins have been the locations where the crust and volatiles sink into the deep Earth's interior. In a generally-accepted arc–trench plate boundary scheme, a subducting slab dehydrates and the dehydrated fluids result in melting of the mantle wedge above the slab producing arc magmas (e.g., Ringwood 1974; Tatsumi et al. 1983). The remnant slab becomes denser and sinks further, crosses the mantle transition zone, and subsequently to the bottom of the lower mantle (e.g., Ringwood 1991). In order to maintain the mass and thermal balances in the entire plate tectonic cycle, oceanic plate subduction is regarded as the subduction input. On the other hand, the major output counterparts are island arc magmas from subduction zones, mid-ocean ridge basalts (MORB) from divergent plate boundaries, and oceanic island basalts (OIB) from hot spots. The detailed mass transfer processes and associated element behaviors between the inputs and the outputs remain unclear. Among those, the outputs from the subducted oceanic plate slab via prograde metamorphism are the key to solve the mass balance issue because of their rigorous dehydration and element transfer back to the surface via arc magmas which clearly contain geochemical slab components (Hermann 2002; Kessel et al. 2005; Kimura 2017; Klimm et al. 2008; Stalder et al. 1998).

To understand the contributions of the slab components to the arc magmas and of the deeply recycled slab residues to the OIBs and MORBs, numerous studies on trace element and isotope geochemistry of basaltic rocks in various tectonic settings have been conducted during the past half a century (e.g., White 1985; Zindler and Hart 1986). Recent accumulations of geochemical data of those magmas allow qualitative discussions on large scale mass circulation throughout the Earth's history (e.g., Kimura et al. 2016). In contrast, geochemical and isotopic data from deeply subducted slab materials are little because of the scarcity of the slab materials on the surface. It is, however, necessary to explore the slab geochemistry in understanding the fate of the subducted

* Corresponding author at: Graduate School of Science, Tohoku University, Aoba, Sendai 980-8578, Japan.
E-mail address: tomomi.hara.r1@dc.tohoku.ac.jp (T. Hara).

https://doi.org/10.1016/j.lithos.2018.09.001
0024-4937/

slab because they provide immediate geochemical records of the subducted slab at a subarc depth.

Lawsonite is a typical Ca-Al hydrous silicate mineral formed under a high-pressure, low-temperature (*HP–LT*) subduction environment. It has a wide stability field (from blueschist to eclogite facies up to ~8–9 GPa and ~830–850 °C in basaltic system, Schmidt and Poli 1998; Okamoto and Maruyama 1999) with large amount of water up to ~11.5 wt% H_2O and is very compatible with many trace elements. Hence, lawsonite is a dominant carrier of water and trace elements in the subducting oceanic crust (cf. Tsujimori et al. 2006a; Tsujimori and Ernst 2014; Martin et al. 2014; Vitale Brovarone and Beyssac, 2014). Lawsonite also supplies trace elements and water to the overriding mantle wedge by its breakdown during lawsonite- to dry-eclogite transformation. As for Sr and Pb, lawsonite crystals in lawsonite-bearing metamorphic rocks contain from 50% to 90% of these elements in the bulk rock compositions (see review by Martin et al. 2014). Consequently, lawsonite is the major carrier of Sr and Pb in the crustal lithologies of the subducting slab. Although subducted oceanic crust is estimated experimentally to transform to lawsonite eclogite from blueschist (e.g., Okamoto and Maruyama 1999; Pawley et al. 1996; Schmidt and Poli 1998), lawsonite occurrence at the surface is scarce because lawsonite is easy to be overprinted during exhumation (Clarke et al. 2006; Tsujimori et al. 2006a; Whitney and Davis 2006).

Numbers of works have reported trace element characteristics of natural lawsonite (e.g., Li et al. 2013; Martin et al. 2014; Spandler et al. 2003; Tribuzio et al. 1996; Ueno 1999; Vitale Brovarone et al. 2014). However, isotopic compositions of lawsonite have not been reported, except for rare Lu-Hf isochron dating of lawsonite (e.g., Mulcahy et al. 2009). In order to reveal the Sr-Pb isotope characteristics of lawsonite and relevant metamorphic processes, we performed an integrated study of petrology and geochemistry of eclogite-facies lawsonite. We employed *in-situ* analytical techniques including a laser ablation inductively coupled plasma mass spectrometry (LA-ICPMS) for major and trace element analyses and a LA-multiple collector inductively coupled plasma mass spectrometry (LA-MC-ICPMS) for Sr and Pb isotope analyses. These techniques allow texture-based geochemical reconnaissance.

We investigated natural lawsonite samples in eclogitic metabasalt and metachert rocks from the South Motagua Mélange (SMM) of the Guatemala Suture Zone (Fig. 1). Lawsonites in those samples are suitable for spot analyses because of their large crystal size (~100–1500 μm in diameter). We mainly analyzed Sr-Pb isotope compositions. Trace and major element analyses of major constituent minerals and the bulk-rock chemical analysis were made on one metabasaltic rock. We discuss trace element distributions in each mineral phase and macro- to micro-scopic isotope variations in the rocks.

Mineral abbreviations in this paper are after Whitney and Evans (2010).

2. Sample descriptions

The sample locality, Carrizal Grande (central Guatemala), is located in a fault-bounded eclogite-bearing serpentinite mélange unit of SMM (e.g., Brueckner et al. 2009; Flores et al. 2013; Harlow et al. 2004; Tsujimori et al., 2005) (Fig. 1). The SMM is one of the geotectonic units consisting the Guatemala Suture Zone, a major left-lateral strike-slip boundary between the North American plate to the north (Maya block) and Caribbean plate (Chortís block) to the south. The SMM eclogites from Carrizal Grande have been known as a L-type lawsonite eclogites (Tsujimori et al. 2006a; Tsujimori and Ernst 2014), which means that prograde-zoned garnet grew only within the lawsonite stability field. Carrizal Grande is also known as a major source of jadeite jade (jadeitite), coexisting with lawsonite eclogites and lawsonite blueschists that are generally found as boulders dismembered from the hosting serpentinite mélange.

The investigated samples include metabasaltic rocks (samples WSB and HJK) and metachert (sample KPT). The metabasaltic rocks are further divided into phengite-rich, glaucophane-free fine-grained lawsonite eclogite (sample WSB) and glaucophane-bearing coarse-grained foliated lawsonite eclogite (sample HJK). According to a definition by Tsujimori et

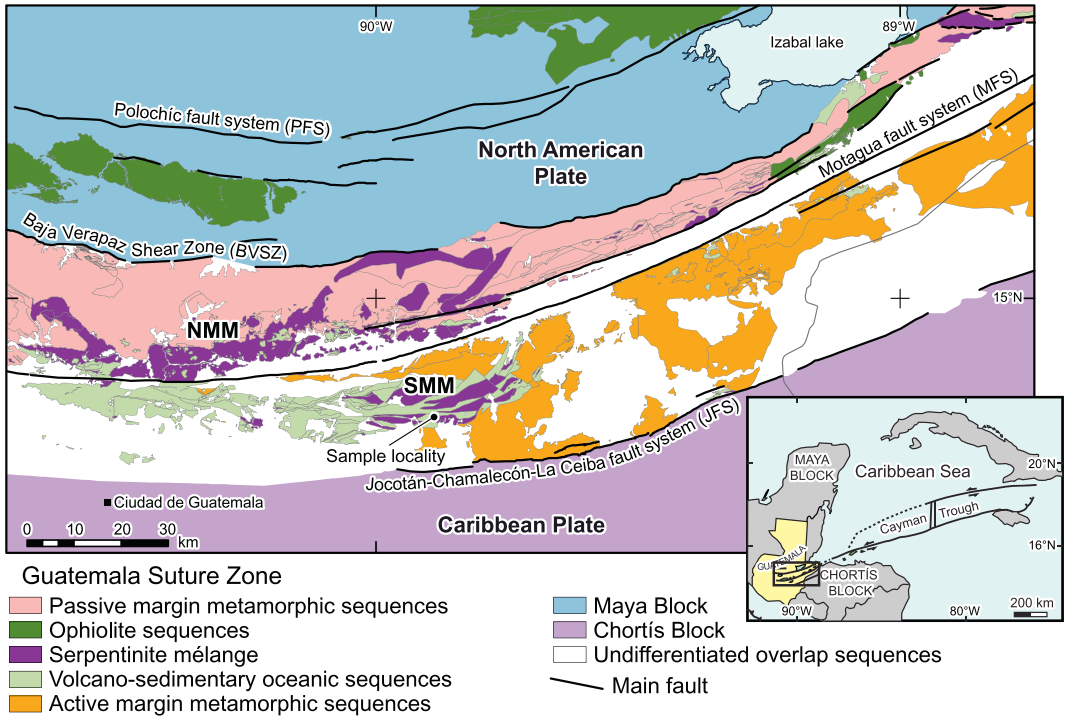

Fig. 1. Geological map of the Guatemala Suture Zone, showing sample locality. The map was modified after Flores et al. (2013) and Harlow et al. (2016). SMM and NMM represent the South Motagua Mélange and North Motagua Mélange, respectively.

al. (2006b), the sample WSB is a phengite-rich variety of Type-I eclogite and the sample HJK belongs to Type-II eclogite of the SMM. The Type-I eclogite preserves an older structure and mineralogy of a prograde eclogite stage, whereas the well-foliated Type-II eclogite records mineralogy and structure during a retrograde eclogite stage. According to Tsujimori et al. (2006b), garnet-clinopyroxene-phengite thermobarometry yields $P = \sim 2.4–2.6$ GPa and $T = \sim 480$ °C for Type-I and $P = \sim 1.8$ GPa and $T = \sim 400$ °C for Type-II eclogites. The protoliths of both WSB and HJK are considered to be oceanic basalts (Tsujimori et al. 2006b). The protolith of KPT would be a pelagic chert overlying oceanic crust. The lawsonite eclogites of SMM yield a Sm-Nd garnet-omphacite-bulk-rock isochron age of ~144–132 Ma (Brueckner et al. 2009). The isochron age was interpreted as a peak eclogite-facies metamorphism.

3. Methods

We prepared polished thick-sections (~180 μm in thickness) of all the samples for LA-ICPMS analyses (Fig. 2). In addition, we also made thin-sections (~30 μm in thickness) for petrographical observations. Textural observations of polished petrographic thin-sections were done by using a JEOL JSM-7001F field emission-scanning electron microscope (FE-SEM). We performed the back-scattered electron (BSE) imaging at a 15 kV acceleration voltage and a 3 nA beam current. Cathodoluminescence (CL) images were observed using a SEM, Hitachi S-3400 N, equipped with a Gatan model MiniCL system. We conducted the CL observation using a 25 kV acceleration voltage and a 90 nA probe current. Bulk-rock analyses of the sample HJK were carried out at Activation Laboratories Ltd., Canada, using Code 4Litho Lithogeochemistry Package. The package uses fusion inductively coupled plasma optical emission spectrometry (FUS-ICPOES) and inductively coupled plasma mass spectroscopy (FUS-ICPMS) for the major and trace element analyses, respectively. Estimation of averaged bulk composition for the sample WSB was done by using JEOL JSM-7001F, equipped with an Oxford INCA X-act Energy EDS system. We estimated the composition by averaging relatively large areal quantitative analyses. Since the sample WSB is petrographically homogeneous, consisting of two major domains, i.e. omphacite-rich and phengite-rich domains, randomly selected 10 sites (approximately 24.3 × 18.3 mm) were analyzed in each domain before the averaging.

The major element compositions of minerals were analyzed by a FE-SEM, JEOL JSM-7001F, equipped with an EDS, Oxford INCA X-act energy dispersive X-ray spectrometer. The quantitative analyses were conducted using a 15 kV acceleration voltage, a 1.4 nA beam current, and a 75 s integration time. In the SEM-EDS analyses, the XPP method (Pouchou et al. 1990) was employed for matrix corrections.

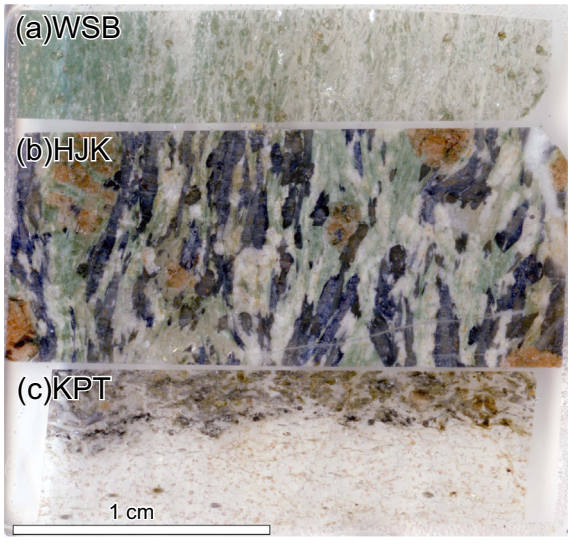

Fig. 2. Scanned image of a composite thick-section including of all the samples for isotope and trace element analyses. (a) Sample WSB (metabasalt). (b) Sample HJK (metabasalt). (c) Sample KPT (metachert).

Concentrations of trace elements of minerals consisting all the samples were analyzed by LA-ICPMS at JAMSTEC; the analysis was performed using an OK Laboratory OK-Fs2000K 266 nm femtosecond laser ablation system with ~12 $J \cdot cm^{-2}$ laser fluence, coupled to a quadrupole ICPMS, Thermo Fisher Scientific iCAP-Q. The spot size was 40 μm in diameter. The background and analysis counting times were 20 and 60 s, respectively. Glass standards provided by the United States Geological Survey (USGS), BHVO-2G was used for the external standardization, and GSD-1G was used for the calibration for every 10 spot analyses. During the trace element analysis, major element compositions were also determined. Details are referred to Kimura and Chang (2012).

The *in-situ* isotope analyses of lawsonites in all the samples were done by LA-MC-ICPMS at JAMSTEC; the analysis was performed using an OK Laboratory OK-EX2000 193 nm nanosecond excimer laser with ~10 $mJ \cdot cm^{-2}$ fluence, coupled to a Thermo Fisher Scientific Neptune MC-ICPMS. Sr isotopic ratios ($^{87}Sr/^{86}Sr$) were determined with the spot size of 100 or 200 μm in diameter and at the repetition rate of 5 or 10 Hz (details are in Table 1). As there were little Rb concentration in lawsonites, calibration for ^{87}Rb overlap on ^{87}Sr was done only at the beginning of the day of analysis. Details are referred to Kimura et al. (2013a). Pb isotopic ratios ($^{206}Pb/^{204}Pb$, $^{207}Pb/^{204}Pb$, $^{208}Pb/^{204}Pb$, $^{207}Pb/^{206}Pb$, $^{208}Pb/^{206}Pb$ and $^{208}Pb/^{207}Pb$) were determined with the spot size of 100 μm in diameter and at the repetition rate of 10 Hz. Mass fractionation calibration was performed using the standard reference glass material SRM 612 provided by the National Institute of Standard and Technology (NIST). We used the average value of the calibration standard measured before and after every unknown spot

Table 1
Sr isotope ratios of lawsonites from all the samples. 2 SE: Error given by 2-standard error.

Spot ID	$^{87}Sr/^{86}Sr$	2 SE	Spot size, μm	Repetition, Hz
WSB-001	0.70355	0.00005	100	5
WSB-002	0.70351	0.00010	100	5
WSB-003	0.70338	0.00012	100	5
WSB-004	0.70349	0.00005	100	5
WSB-005	0.70346	0.00008	100	5
WSB-006	0.70341	0.00008	100	5
WSB-056	0.70343	0.00015	100	5
WSB-057	0.70335	0.00015	100	5
WSB-058	0.70339	0.00015	100	5
WSB-059	0.70346	0.00008	100	5
WSB-060	0.70349	0.00011	100	5
HJK-007	0.70646	0.00010	100	5
HJK-008	0.70572	0.00007	100	5
HJK-009	0.70594	0.00008	100	5
HJK-010	0.70586	0.00006	100	5
HJK-011	0.70662	0.00012	100	5
HJK-012	0.70648	0.00012	100	5
HJK-013	0.70577	0.00010	100	5
HJK-014	0.70568	0.00007	100	5
HJK-015	0.70601	0.00008	100	5
HJK-016	0.70660	0.00019	100	5
HJK-050	0.70558	0.00013	100	5
HJK-051	0.70601	0.00013	100	10
HJK-052	0.70636	0.00015	100	5
HJK-053	0.70596	0.00012	100	5
HJK-054	0.70574	0.00008	100	5
HJK-055	0.70651	0.00013	100	5
KPT-017	0.70564	0.00006	100	5
KPT-018	0.70743	0.00015	100	5
KPT-019	0.70697	0.00015	100	5
KPT-020	0.70708	0.00010	100	10
KPT-021	0.70752	0.00005	100	10
KPT-022	0.70750	0.00007	100	10
KPT-023	0.70734	0.00005	100	10
KPT-024	0.70757	0.00004	100	10

analysis. Error propagation was considered based on the 2-standard errors for two calibration standards and an unknown. Details are referred to Kimura et al. (2013b).

4. Result

4.1. Petrography

Sample WSB is a foliated, phengite-rich, glaucophane-free fine-grained lawsonite eclogite (Fig. 2a). It shows compositional banding defined by omphacite-rich and phengite-rich domains. Lawsonite-rich subdomains, aligning parallel to a schistosity, are also identified (Fig. 3a). Lawsonite occurs as euhedral to subhedral grains with rectangular shapes (100–200 μm in length) and is scattered in the matrix. Garnet porphyroblasts, up to 300 μm in diameter, are scattered in a foliated matrix. Garnets are partially replaced by chlorite along fractures (Fig. 3b). Phengite is oriented parallel to the schistosity.

Sample HJK is a glaucophane-bearing, coarse-grained foliated lawsonite eclogite (Fig. 2b). It is composed of omphacite, glaucophane, garnet, and lawsonite, with minor rutile, titanite, phengite, chlorite, and quartz. Major constituent minerals in the sample reach up to ~1 mm in length and most of them can be recognized by the naked eye. Prismatic lawsonite reaches up to 2 mm in length; it is twinned and contains inclusions of rutile and rare zircon (Fig. 3c). Secondary titanite replaces rutile in the matrix and contains abundant mineral inclusions. Garnet porphyroblasts (1–3 mm in diameter) contain inclusions of tiny lawsonite and rutile. The latest stage crack-sealing albite veins are developed in the matrix (Fig. 3d).

Sample KPT is a garnet- and phengite-bearing quartzite (Fig. 2c). It is schistose and heterogeneous composed of lawsonite-free and lawsonite-rich layers (Figs. 2, 3e); the boundary of these two layers is sharp. A penetrative schistosity is defined by the preferred orientation of phengite. Lawsonite-free layer consists of quartz with small euhedral garnet (~15 μm in diameter) and phengite, whereas lawsonite-rich layer also contains lawsonite and glaucophane. Lawsonite exhibits resorption forms, 0.5–1.5 mm in length (Figs. 3e, f). Garnet in the lawsonite-rich layer reaches up to ~1.5 mm in length. Rutile, zircon and secondary titanite are found as accessory phases only in lawsonite-rich layer.

4.2. Bulk rock compositions

Table 2 shows the bulk-rock major and trace element concentrations of the sample HJK. The sample HJK has a basaltic bulk-rock composition with $SiO_2 = 50.3$ wt%, $Al_2O_3 = 15.7$ wt%, $FeO^* = 9.3$ wt%, $TiO_2 = 1.7$ wt%, and $P_2O_5 = 1.4$ wt% (total Fe reported as FeO^*). Minimum water content based on the LOI (loss-on-ignition) is 3.5 wt%. The enrichment

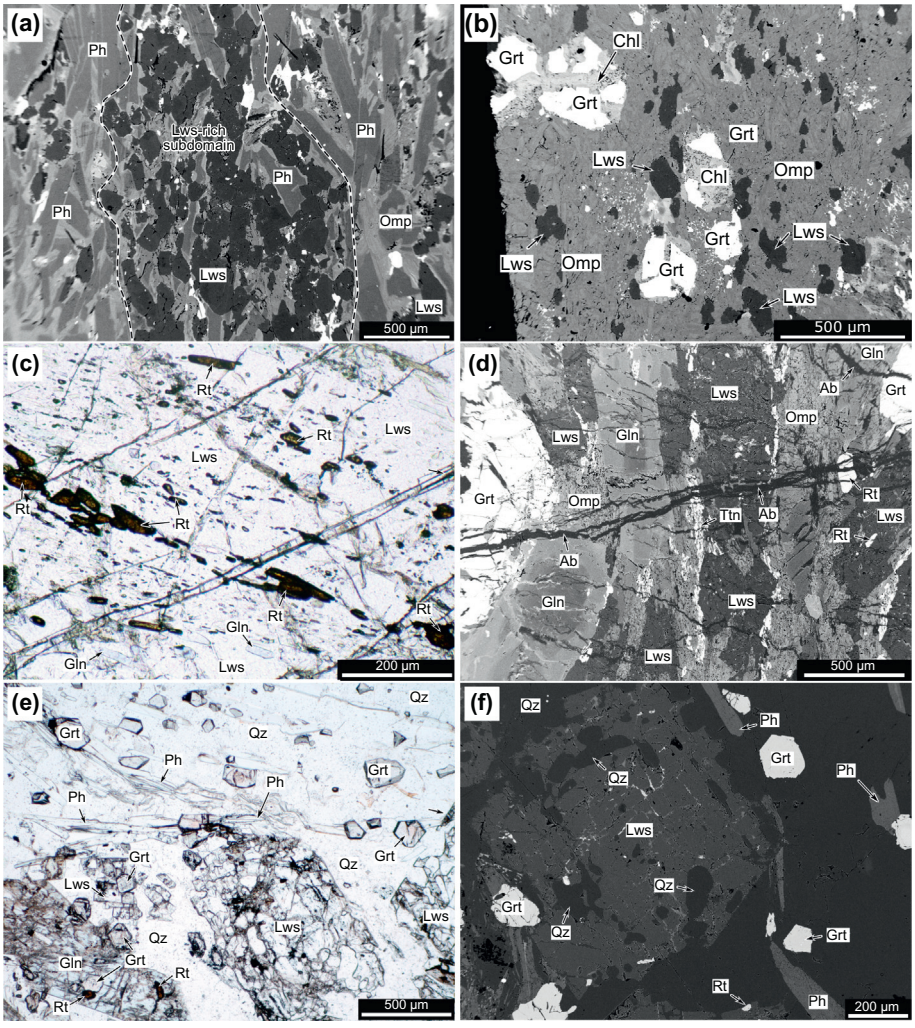

Fig. 3. Representative microtextures. (a) Back-scattered electron (BSE) image showing a lawsonite-rich subdomain in a phengite-rich domain in the sample WSB. (b) BSE image showing occurrence of lawsonite in an omphacite-rich domain in the sample WSB. (c) Plane polarized light (PPL) image of eclogite-facies lawsonite containing rutile inclusions. (d) BSE image showing many fine albite veins cutting coarse-grained minerals in the sample HJK. (e) PPL image showing a lawsonite-free layer (upper half of the photo) and lawsonite-bearing layer (lower half) in the sample KPT. (f) BSE image showing a coarse-grained lawsonite with resorption texture in the sample KPT.

Table 2
Bulk-rock composition of the sample HJK.

SiO_2	50.33
Al_2O_3	15.73
FeO*	9.29
MnO	0.122
MgO	5.11
CaO	6.83
Na_2O	4.15
K_2O	0.98
TiO_2	1.648
P_2O_5	0.14
LOI	3.51
Total	98.86
Sc	38
Be	< 1
V	266
Cr	310
Co	48
Ni	160
Cu	90
Zn	170
Ga	17
Ge	1.3
As	< 5
Rb	25
Sr	315
Y	28.8
Zr	119
Nb	5.8
Mo	< 2
Ag	0.5
In	< 0.1
Sn	< 1
Sb	0.2
Cs	1
Ba	425
La	8.75
Ce	21.4
Pr	3.13
Nd	16
Sm	4.87
Eu	1.69
Gd	6
Tb	0.9
Dy	5.44
Ho	1.13
Er	3.05
Tm	0.452
Yb	2.85
Lu	0.428
Hf	2.6
Ta	0.39
W	1.1
Tl	< 0.05
Pb	5
Bi	< 0.1
Th	0.43
U	0.21

LOI: Loss of Ignition

of Na_2O (4.2 wt%) might be gained during seafloor hydrothermal alteration or metasomatism. Relationship of Nb/Y (0.2) – Ti/Y (340) suggests a MORB-like affinity (Pearce et al. 1984). CI-chondrite-normalized rare earth element (REE) pattern of the sample HJK is relatively flat, but light (L)REEs are enriched (Fig. 4a).

Primitive mantle (PM)-normalized trace elements pattern of the sample HJK is also shown in Fig. 4b. The pattern shows relative enrichment of large ion lithophile elements (LILEs) (Rb, Ba, and Sr), LREEs and Pb, Th and U. Hf is depleted relative to Nd and heavy (H)REEs. Pb shows a strong positive spike, suggesting elevated partition coefficient in lawsonite and possible addition from sedimentary components. Estimated averaged bulk-rock major element composition of the sample WSB is also basaltic with SiO_2 = 49.2 wt%, Al_2O_3 = 23.7 wt%, FeO* = 5.4 wt% and TiO_2 = 1.4 wt%. Observed high K_2O (4.1 wt%) suggests a significant modification (metasomatic potassium addition) during eclogite-facies metamorphism. The compositions of both HJK and WSB are plotted in the ACF diagram (Fig. 5); where A = Al_2O_3 + Fe_2O_3 – [Na_2O + K_2O], C = CaO, and F = FeO + MgO (molar composition). In the ACF diagram, the sample HJK is plotted within three-phase triangle of garnet (Grt) + lawsonite (Lws) + omphacite (Omp). This is consistent with the lack of glaucophane in the sample WSB.

4.3. Mineral compositions

Major and trace element compositions of major mineral phases analyzed are listed in Tables S1–S7.

4.3.1. Sample WSB

Lawsonite contains ~1312–2683 μg/g Sr, ~4.6–19.6 μg/g Pb, ~0.22–5.85 μg/g Th and ~0.11–0.30 μg/g U (Table S2). Pb content in lawsonite is lower than other samples. Lawsonite shows a LREE-enriched and HREE-depleted CI-chondrite-normalized REE patterns that suggests crystallization coeval with garnet (Fig. 6a). LREE concentrations are four orders of magnitude larger than those of the coexisting garnet. HREEs abundance of lawsonite in the sample WSB is slightly higher than those of the other samples. The PM-normalized trace element pattern shows enrichment of U, Th and Pb (Fig. 6b). Garnet has a composition of pyrope $(Pyr)_{3.5–8.0}$ almandine $(Alm)_{64–73}$ grossular $(Grs)_{17–20}$ spessartine $(Sps)_{1.9–13}$. Garnet is depleted in LREEs and enriched in mid (M)REEs and HREEs (Fig. 6c). The garnet core has higher HREEs than in the rim. Phengite has a flat REE pattern but shows a positive Eu anomaly, and in the multi element plot diagram, phengite shows very high concentrations of Rb and Ba (Fig. 6f).

4.3.2. Sample HJK

Lawsonite contains ~951–3528 μg/g Sr, ~16.8–58.6 μg/g Pb, ~0.04–36.07 μg/g Th and ~0.02–2.38 μg/g U (Table S1). Some lawsonites have high Zr and Hf contents. They are probably contaminated by small zircon inclusions within the lawsonites. Lawsonite has compositional zonings of trace elements; they are enriched in the core. Lawsonite has a LREE-enriched and HREE-depleted REE pattern that suggests crystallization coeval with garnet (Fig. 6a). The multi element plot diagram shows enrichment of U, Th and Pb (Fig. 6b).

Garnet has a composition of $Pyr_{13–16}$ $Alm_{63–65}$ $Grs_{18–20}$ $Sps_{1.0–4.5}$. Garnet is depleted in LREEs and enriched in MREEs and HREEs (Fig. 6c). Omphacite contains a composition of jadeite $(Jd)_{42–55}$ aegirine $(Ae)_{3.3–9.0}$ augite $(Aug)_{38–49}$. The REE pattern of omphacite is relatively flat (Fig. 6g). HREE concentrations are two orders of magnitude smaller than those of the coexisting garnet. Glaucophane has remarkable chemical zoning of Fe and Mg; Fe and Mg are enriched in the rim and the core, respectively (Tables S5, S6). The REE pattern of glaucophane is relatively flat (Fig. 6i). The REE concentrations are one order of magnitude smaller than those of the omphacite. Phengite has a flat REE pattern but shows a positive Eu anomaly, and the multi element plot diagram shows very high concentrations of Rb and Ba (Fig. 6f).

4.3.3. Sample KPT

Lawsonite contains ~1416–1611 μg/g Sr, ~62.5–141.8 μg/g Pb, ~2.80–27.48 μg/g Th and ~0.39–7.32 μg/g U (Table S2). Lawsonite contains higher Pb than that of other samples. This is consistent with previous studies that lawsonites in metasedimentary rocks show higher Pb content than those in metabasaltic rocks because there are fewer phases compete for trace elements than in metabasaltic rocks (Martin et al. 2014; Spandler et al. 2003). Lawsonite core has higher trace element concentrations as the sample HJK. The CL images did not confirm zoning in lawsonite. Lawsonite has a LREE-enriched and HREE-depleted REE pattern that suggests crystallization coeval with garnet (Fig. 6a). The trace element pattern shows enrichment of U, Th, and Pb (Fig. 6b).

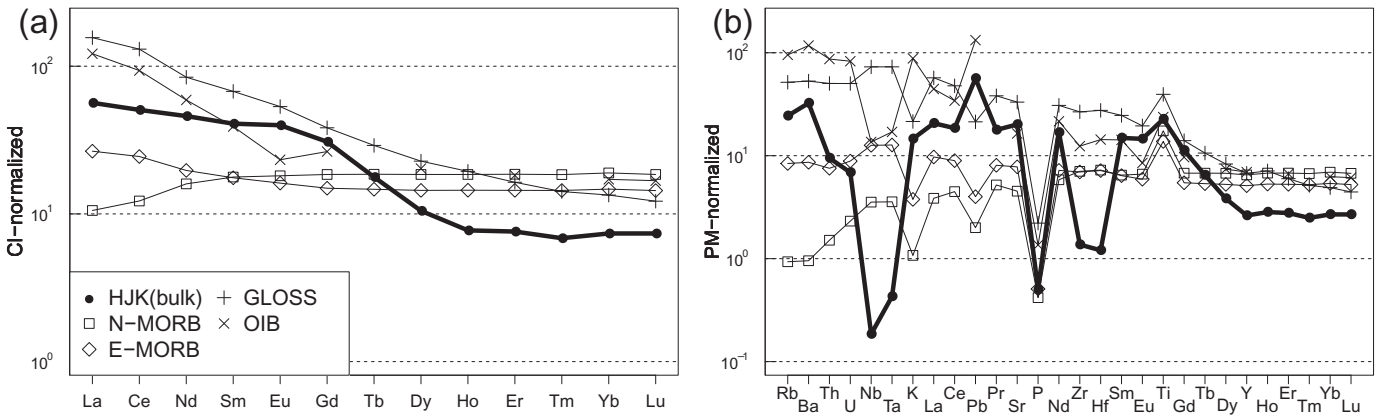

Fig. 4. REEs and trace element patterns of bulk-rock composition of the sample HJK. (a) CI-chondrite normalized REEs concentration. (b) Primitive Mantle (PM)-normalized trace elements concentration. For comparison, reference values of N-MORB, *E*-MORB, OIB by Sun and McDonough (1989), and Global Subducting Sediment (GLOSS) by Plank and Langmuir (1998) are also shown. Normalization factors are from McDonough and Sun (1995).

Garnet has a composition of $Pyr_{6.0–12}$ $Alm_{47–66}$ $Grs_{10–30}$ $Sps_{0.8–31}$. Garnet is depleted in LREEs and enriched in MREEs and HREEs (Fig. 6c). The MREEs and HREEs show relatively flat pattern. Glaucophane has a relatively flat REE pattern (Fig. 6i). Phengite also has a flat REE pattern but shows a positive Eu anomaly, and the multi element plot diagram shows very high concentrations of Rb and Ba (Fig. 6f). An analyzed spot of a phengite next to a lawsonite probably contained a LREE-rich mineral existed at the edge of the lawsonite (phe1 of KPT in Table S7).

4.4. Isotopic ratios of lawsonite

4.4.1. Sr (^{87}Sr-^{86}Sr) isotopes

Strontium isotope ratios ($^{87}Sr/^{86}Sr$) of lawsonite crystals are listed in Table 2 and shown in a histogram in Fig. 7. In the sample WSB, the lawsonite crystals have the relatively low $^{87}Sr/^{86}Sr$ ratios with a very small variation, $^{87}Sr/^{86}Sr = 0.70335–0.70355$. These values are similar to a reference MORB value ($^{87}Sr/^{86}Sr$ = ~0.7022–0.7040, Workman and Hart 2005) and are consistent with the basaltic protolith. In the sample HJK, coarse-grained lawsonite crystals have higher $^{87}Sr/^{86}Sr$ ratios than MORB and show isotopic zoning. The lawsonite cores have $^{87}Sr/^{86}Sr = 0.70558–0.70601$ and the ratios increase at the rims ($^{87}Sr/^{86}Sr = 0.70636–0.70662$). The isotopic zoning shows a compositional gap rather than gradual change. The isotopic variations at both the cores and the rims are relatively small. Although the protolith of the sample HJK was probably basaltic, the Sr isotope ratios are higher, completely out of the MORB field. In the sample KPT, lawsonite crystals have higher isotope ratios and show small isotopic variation especially at the rims. Except for a few rim data, however, most of the isotope ratios are homogeneous ($^{87}Sr/^{86}Sr$ ratios = 0.70697–0.70757). One spot, KPT-017, shows significantly lower value ($^{87}Sr/^{86}Sr = 0.70564$) relative to other spots in the same sample. Note that the lawsonites in the sample KPT contain tiny inclusions of LREE-rich minerals (e.g., allanite) and are also fractured possibly suggesting effect of secondary alteration. The apparent isotopic variation is likely caused by contamination of tiny Sr-rich secondary minerals ablated within the laser spot.

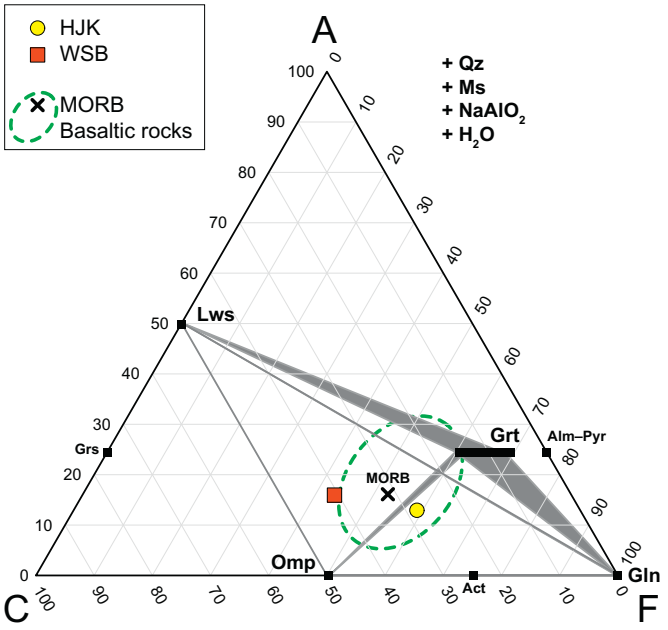

Fig. 5. ACF diagram showing a bulk-rock composition of the samples HJK ($A = Al_2O_3 + Fe_2O_3 - [Na_2O + K_2O]$, $C = CaO$, and $F = FeO + MgO$). For comparison, an inferred average bulk-rock composition based on SEM-EDS analyses of sample WSB is also plotted.

4.4.2. Pb (^{206}Pb,^{207}Pb,^{208}Pb, and^{204}Pb) isotopes

Lead isotope ratios ($^{206}Pb/^{204}Pb$, $^{207}Pb/^{204}Pb$, $^{208}Pb/^{204}Pb$, $^{207}Pb/^{206}Pb$, and $^{208}Pb/^{206}Pb$) of lawsonite crystals are listed in Table 3. All data are shown in Fig. 8. In the sample WSB, lawsonites show minor variations in the Pb isotope ratios, $^{207}Pb/^{206}Pb = 0.8401–0.8512$ and $^{208}Pb/^{206}Pb = 2.0757–2.0911$. It is likely that the isotopic variations reflect the inter-crystal isotope fractionations caused by diffusion. However, core–rim analyses in one lawsonite grain suggests no significant variation in a single crystal; the spots WSB003 (rim) and WSB004 (core) had similar isotopic composition ($^{207}Pb/^{206}Pb =$ 0.8501 [rim], 0.8510 [core], and $^{208}Pb/^{206}Pb = 2.0777$ [rim], 2.0790 [core]) (Table 3). Those values overlap within analytical uncertainties. This strongly suggests that the isotopic variations in the sample WSB is not attributed to the isotopic diffusion during lawsonite growth. In the sample HJK, as same as Sr isotope, Pb isotope ratios show core–rim zonation. The lawsonite cores show MORB-like values of $^{207}Pb/^{206}Pb$ = ~0.843–0.844 (Workman and Hart 2005), whereas the rims show enriched compositions $^{207}Pb/^{206}Pb$ = ~0.839–0.841.

In the sample KPT, Pb isotope ratios of lawsonites show a wider variation. Some extreme values might have been derived from contamination of tiny Pb-rich minerals in the analytical spots. Non-zoned lawsonites show a relatively homogeneous composition $^{208}Pb/^{206}Pb$ = ~2.07.

4.5. Age-corrected Pb isotopes

Since $^{206–208}Pb$ are radiogenic and the lawsonites contain considerable amount of U and Th, the Pb isotope ratios should have grown with time due to radioactive decay of the parent isotopes. In contrast, Rb content in lawsonite is almost negligible; it is not necessary to consider age

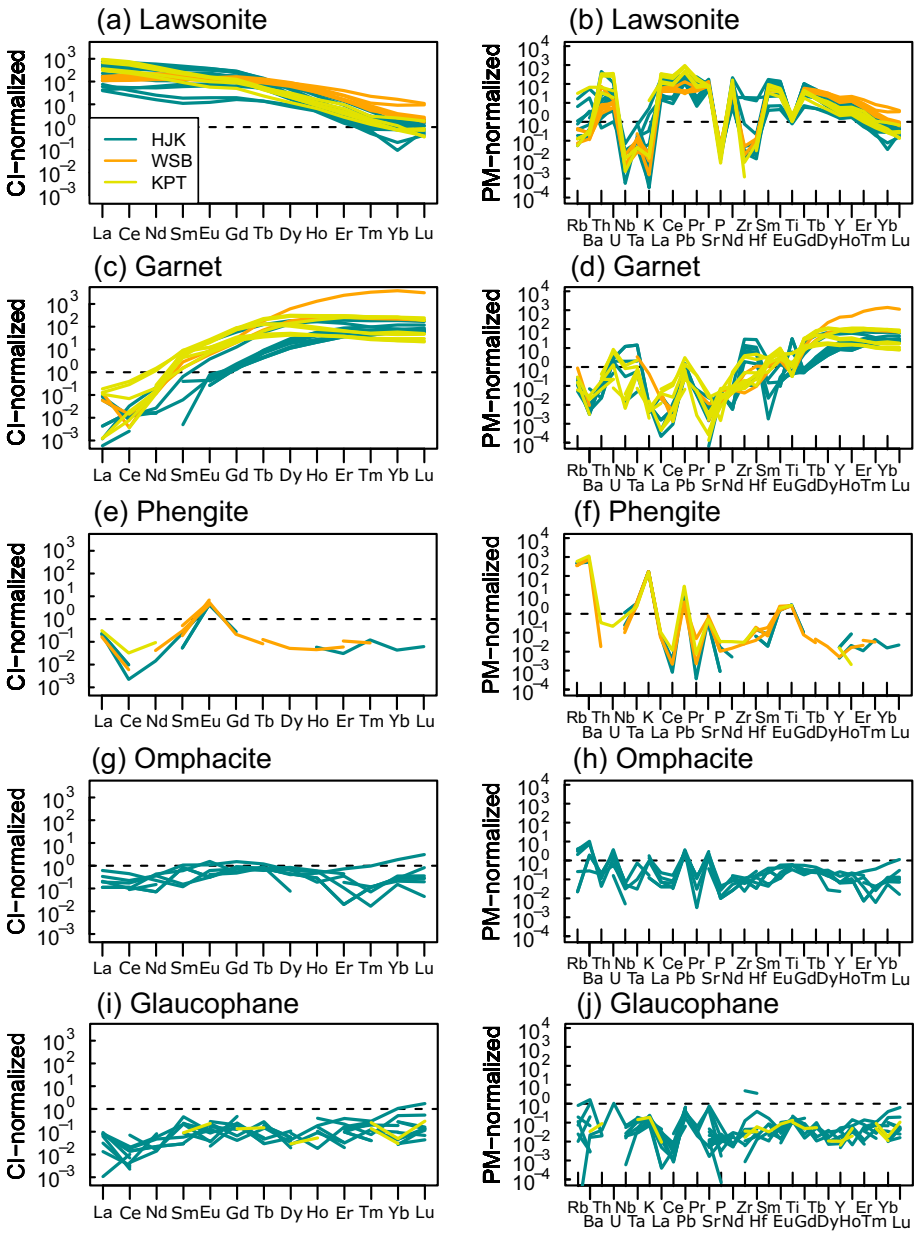

Fig. 6. CI-normalized REEs and PM-normalized trace elements abundances of various minerals. (a) REE patterns of lawsonites. (b) Trace element patterns of lawsonites. (c) REE patterns of garnets. (d) Trace element patterns of garnets. (e) REE patterns of phengites. (f) Trace element patterns of phengites. (g) REE patterns of omphacites. (h) Trace element patterns of omphacites. (i) REE patterns of glaucophanes. (j) Trace element patterns of glaucophanes. Both normalization factors are from McDonough and Sun (1995).

corrections for ^{87}Sr isotope. Metamorphic ages of the Guatemalan lawsonite eclogites are ~144–132 Ma (Brueckner et al. 2009), so nominal ages of 100, 150 and 200 Ma were examined for all the samples. Concentrations of U, Th and Pb were estimated by the data from the nearest spot of the isotope ratio analyses. The concentrations were averaged in each grain (or crystal) for the rims and the cores. Note that the analyzed lawsonites in the sample WSB for trace elements were different crystals from that for Pb isotopes; therefore, all the trace element data were averaged and applied. For the sample KPT, only one crystal was analyzed for trace elements; therefore, both the rim and the core data from the crystal were adopted to all others. For the age correction calculations, we adopted several assumptions: (1) total natural abundance of ^{204}Pb, ^{206}Pb, ^{207}Pb and ^{208}Pb is 1; (2) total natural abundance of ^{235}U and ^{238}U is 1, and isotope ratio of ^{238}U/^{235}U today is 137.88 (Rosman and Taylor 1998); (3) natural abundance of ^{232}Th is 1. From each Pb isotope analysis (Table 3), abundance of each Pb isotope can be calculated. Initial ^{206}Pb/^{204}Pb, ^{207}Pb/^{204}Pb and ^{208}Pb/^{204}Pb were calculated by the decay constant of $\lambda^{238} = 1.55125 \times 10^{-10}$ for ^{238}U, $\lambda^{235} = 9.8485 \times 10^{-10}$ for ^{235}U and $\lambda^{232} = 4.9475 \times 10^{-11}$ for ^{232}Th (Jaffey et al. 1971) and by the nominal correction ages mentioned above. Initial ^{207}Pb/^{206}Pb and ^{208}Pb/^{206}Pb were obtained by the ratios of the above calculation results. Since U and Th contents are given by three effective digits (significant figures), the effective digits of all

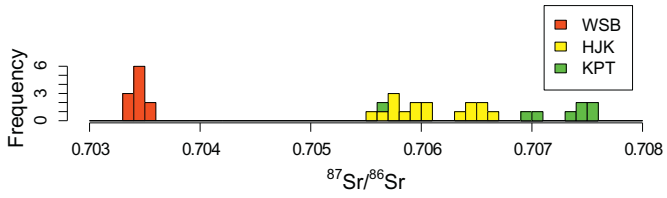

Fig. 7. Histogram showing ^{87}Sr/^{86}Sr of lawsonites. Lawsonite in the sample HJK has Sr isotope zoning (see details in text).

Table 3
Pb isotope ratios of lawsonites from all the samples. All the analyses were performed with the spot size of 100 μm in diameter and at the repetition rate of 10 Hz. 2 SE: Error given by 2-standard error.

spot ID	$^{206}Pb/^{204}Pb$	2 SE	$^{207}Pb/^{204}Pb$	2 SE	$^{208}Pb/^{204}Pb$	2 SE	$^{207}Pb/^{206}Pb$	2 SE	$^{208}Pb/^{206}Pb$	2 SE	$^{208}Pb/^{207}Pb$	2 SE
WSB-001	18.29	0.05	15.54	0.04	38.16	0.09	0.8492	0.0009	2.0857	0.0003	2.4563	0.0012
WSB-002	18.39	0.06	15.57	0.05	38.14	0.11	0.8472	0.0009	2.0762	0.0005	2.4505	0.0006
WSB-003	18.17	0.08	15.47	0.07	37.76	0.18	0.8501	0.0008	2.0777	0.0006	2.4437	0.0008
WSB-004	18.23	0.09	15.50	0.07	37.88	0.17	0.8510	0.0008	2.0790	0.0007	2.4429	0.0014
WSB-005	18.32	0.07	15.55	0.05	38.09	0.15	0.8498	0.0007	2.0790	0.0006	2.4459	0.0015
WSB-006	18.31	0.07	15.57	0.06	38.06	0.15	0.8502	0.0007	2.0787	0.0004	2.4449	0.0010
WSB-007	18.30	0.12	15.57	0.10	38.03	0.24	0.8512	0.0007	2.0791	0.0005	2.4423	0.0015
WSB-008	18.38	0.09	15.61	0.07	38.15	0.19	0.8494	0.0009	2.0757	0.0007	2.4435	0.0010
WSB-009	18.30	0.05	15.56	0.04	38.04	0.11	0.8500	0.0006	2.0778	0.0004	2.4446	0.0007
WSB-010	18.51	0.08	15.56	0.04	38.71	0.16	0.8401	0.0007	2.0911	0.0020	2.4891	0.0058
WSB-011	18.41	0.05	15.59	0.04	38.25	0.10	0.8468	0.0006	2.0787	0.0006	2.4547	0.0015
HJK-012	18.59	0.03	15.62	0.03	38.48	0.06	0.8403	0.0005	2.0693	0.0004	2.4626	0.0005
HJK-013	18.56	0.03	15.60	0.02	38.38	0.05	0.8409	0.0003	2.0688	0.0004	2.4603	0.0005
HJK-014	18.50	0.05	15.61	0.04	38.33	0.10	0.8440	0.0003	2.0727	0.0004	2.4558	0.0005
HJK-015	18.52	0.05	15.62	0.04	38.38	0.10	0.8433	0.0003	2.0722	0.0003	2.4571	0.0005
HJK-016	18.60	0.04	15.63	0.03	38.49	0.08	0.8401	0.0004	2.0694	0.0003	2.4631	0.0004
HJK-017	18.62	0.03	15.63	0.03	38.51	0.07	0.8396	0.0004	2.0685	0.0003	2.4634	0.0004
HJK-018	18.62	0.03	15.62	0.02	38.46	0.06	0.8388	0.0006	2.0659	0.0003	2.4627	0.0005
HJK-019	18.60	0.04	15.63	0.03	38.47	0.08	0.8402	0.0003	2.0680	0.0003	2.4611	0.0004
HJK-020	19.19	0.11	15.67	0.04	38.74	0.11	0.8164	0.0072	2.0180	0.0035	2.4709	0.0015
HJK-021	18.59	0.05	15.61	0.03	38.42	0.08	0.8404	0.0004	2.0677	0.0004	2.4606	0.0008
HJK-022	18.50	0.05	15.60	0.04	38.33	0.10	0.8429	0.0004	2.0713	0.0004	2.4567	0.0010
HJK-023	18.58	0.05	15.62	0.04	38.44	0.11	0.8411	0.0004	2.0697	0.0004	2.4608	0.0012
HJK-024	18.51	0.03	15.62	0.02	38.36	0.06	0.8438	0.0003	2.0727	0.0003	2.4561	0.0005
KPT-025	18.65	0.04	15.64	0.03	38.61	0.07	0.8385	0.0002	2.0698	0.0003	2.4685	0.0004
KPT-026	18.68	0.03	15.64	0.02	38.65	0.06	0.8369	0.0002	2.0687	0.0003	2.4717	0.0003
KPT-027	19.42	0.18	15.66	0.02	38.57	0.07	0.8073	0.0200	1.9898	0.0076	2.4646	0.0016
KPT-028	18.60	0.03	15.63	0.02	38.49	0.06	0.8409	0.0003	2.0702	0.0003	2.4619	0.0004
KPT-029	18.65	0.02	15.63	0.02	38.58	0.05	0.8380	0.0003	2.0691	0.0004	2.4690	0.0003
KPT-030	18.73	0.05	15.64	0.03	38.51	0.07	0.8359	0.0025	2.0578	0.0011	2.4615	0.0004
KPT-031	18.59	0.04	15.60	0.03	38.45	0.08	0.8394	0.0003	2.0685	0.0004	2.4643	0.0004
KPT-032	18.59	0.03	15.63	0.02	38.48	0.06	0.8408	0.0003	2.0703	0.0004	2.4624	0.0004
KPT-033	18.69	0.04	15.64	0.03	38.86	0.11	0.8370	0.0014	2.0799	0.0003	2.4851	0.0019
KPT-034	18.72	0.04	15.65	0.03	38.93	0.08	0.8361	0.0005	2.0795	0.0003	2.4873	0.0006
KPT-035	18.68	0.03	15.64	0.02	38.59	0.07	0.8374	0.0003	2.0659	0.0004	2.4671	0.0005

results are three. The results of calculations are summarized in Tables S8 and S9. As shown in Fig. S2, all the corrected isotope ratios were not significantly different from non-corrected values, because of the low concentrations of U and Th relative to Pb.

5. Discussion

5.1. Elemental mass balance

We evaluated elemental mass balance using *in-situ* trace elements data of the five major minerals (glaucophane, omphacite, lawsonite, garnet and phengite) and a bulk-rock trace element composition of the sample HJK. Relative modal weight composition of the sample HJK is 40.6% glaucophane, 25.6% omphacite, 19.0% lawsonite, 9.0% garnet, 4.0% phengite and others (trace amounts of secondary ~1% albite, ~0.5% titanite and ~0.3% apatite). The calculated elemental mass balance is visualized in Fig. 9. As shown, most LREEs, Sr, Pb, Th and U are accommodated in lawsonite. This result is consistent with that in the previous studies for a blueschist-facies metabasaltic rock from New Caledonia by Spandler et al. (2003) and an eclogite-facies metasomatic rock from Corsica (France) and an eclogite-facies impure quartzite from Sivrihisar (Turkey) by Martin et al. (2014). Although we did not consider zircon for the calculations, the total sum of Zr and Hf in minerals is almost consistent with their abundance in bulk-rock. This suggests the presence of sub-micron size zircon in lawsonite, glaucophane, and garnet ablated with the host minerals. In the mass balance estimation, total amounts of some specific elements, especially Nb and HREEs, are larger than those of the bulk. This also suggests that the titanite inclusions were ablated with the host minerals and might be caused by over estimation of the modal weight of garnet. In contrast, depletion of total amounts of Rb and Ba was caused by underestimation of the modal weight of phengite.

5.2. Sr-Pb isotope systematics of lawsonite: A case of South Motagua Mélange

5.2.1. Sr-Pb isotope characteristics of lawsonite

The investigated all Motagua Mélange samples represent a rock suite derived from the same subduction zone. Nevertheless, the Sr-Pb isotope compositions are different between the samples, reflecting their different protoliths. In Fig. 10, all isotope data obtained in this study are plotted along with the compositional field of MORB. As shown in the $^{87}Sr/^{86}Sr$ versus $^{206}Pb/^{204}Pb$ and $^{208}Pb/^{204}Pb$ versus $^{206}Pb/^{204}Pb$ spaces, the sample WSB is isotopically very similar to MORB, whereas the other two samples HJK and KPT are out of the MORB fields especially in terms of Sr isotopes. As described above, the sample HJK has basaltic major element composition similar with WSB. Therefore, the original Sr isotope composition in the sample HJK might have been completely modified. The Sr isotope ratios of the sample KPT, which has a pelagic chert protolith suggested by its field occurrence and the mineralogical features, overlaps the seawater value at ~140 Ma ($^{87}Sr/^{86}Sr$ = ~0.7075, Veizer et al. 1999). This suggests that the isotopic compositions of the pelagic chert reflect seawater value rather than sediments ($^{87}Sr/^{86}Sr$ = ~0.71730, Plank and Langmuir 1998). Although isotope ratios of the pelagic chert may be easily modified from the seawater value by mixing with the terrigenous influxes, the Sr isotope ratio of the sample KPT still preserves the seawater value at the time of deposition. The sample KPT may represent the isotopic compositions of

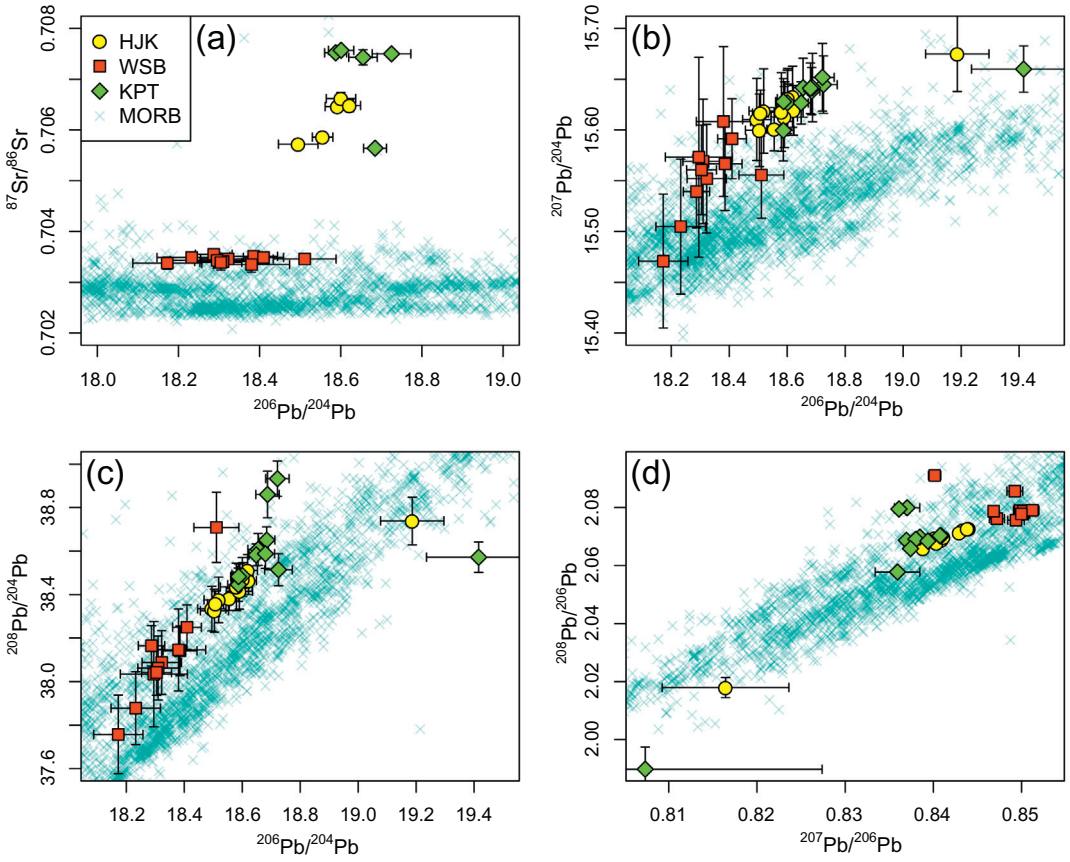

Fig. 8. Binary plots showing Sr-Pb isotopes of lawsonites. Data for MORB were downloaded from the PetDB Database (http://www.earthchem.org/petdb) on 3 July 2018, using following parameter: tectonic setting = SPREADING_CENTER. (a) $^{206}Pb/^{204}Pb$ versus $^{87}Sr/^{86}Sr$ diagram. (b) $^{206}Pb/^{204}Pb$ versus $^{207}Pb/^{204}Pb$ diagram. (c) $^{206}Pb/^{204}Pb$ versus $^{208}Pb/^{204}Pb$ diagram. (d) $^{207}Pb/^{206}Pb$ versus $^{208}Pb/^{206}Pb$ diagram. Lawsonite in the sample HJK has Sr isotope zoning (see details in text). Note that due to small natural abundance of ^{204}Pb (~0.014), errors of $^{206}Pb/^{204}Pb$, $^{207}Pb/^{204}Pb$ and $^{208}Pb/^{204}Pb$ are larger than that of $^{207}Pb/^{206}Pb$ and $^{208}Pb/^{206}Pb$.

seawater at ~140 Ma, not only for Sr isotopes but also for Pb isotopes which are not available in the literature. This study suggests isotope ratios of $^{87}Sr/^{86}Sr = 0.70697–0.70757$ and $^{208}Pb/^{206}Pb = ~2.07$ for the seawater at ~140 Ma. Note that Sr isotope ratio is almost homogeneous over the ocean in the world, but Pb isotope ratios are different depending on localities (Frank 2002).

It is also possible that the metachert was partially affected by a GLOSS-like sedimentary component during metamorphism. However, quartz-dominant lithological feature of metachert suggests that the mixing effect of a GLOSS-like component with high Sr abundance (>10 times higher than pelagic chert in general) into the sample KPT was very small.

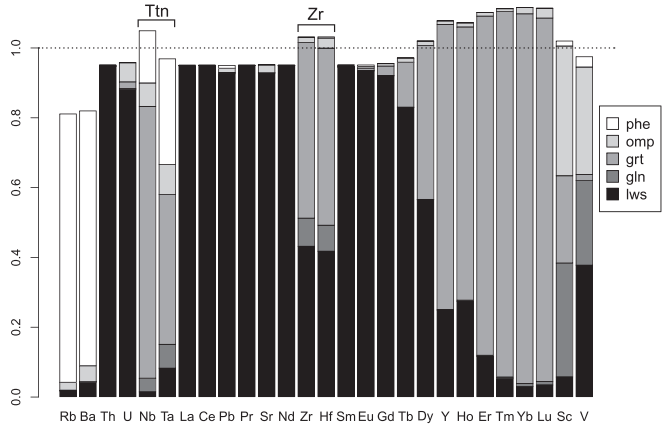

Fig. 9. Trace element budgets of five major minerals (glaucophane, omphacite, lawsonite, garnet and phengite) of the sample HJK. Each trace element was normalized by the bulk composition of the sample HJK (Table 1).

5.2.2. Isotopic modification of metabasaltic rock by seawater

The sample HJK has a basaltic major element composition. However, bulk-rock trace element geochemistry suggests a significant modification by seafloor alteration or fluid-mediated metasomatism during subduction. As shown in Fig. 10a, the Sr isotope ratios of lawsonites in the sample HJK ($^{87}Sr/^{86}Sr$ at the cores = 0.70558–0.70601, $^{87}Sr/^{86}Sr$ at the rim = 0.70636–0.70662) are also different from a MORB-like trend. These values are rather similar to those of metachert. It has been known that the seawater is enriched in Sr relative to CI-chondrite (McDonough and Sun 1995). Considering high Sr concentration in the seawater (~7.6 μg/g in deep seawater, Frank 2002), a water (seawater)–rock (basalt) interaction before subduction zone metamorphism would be a plausible mechanism to modify the Sr isotope values from the original basaltic rock (e.g., Hirahara et al. 2015). The modification of Sr by a seawater–oceanfloor rock interaction is also supported by enrichment of Na_2O.

5.3. Significance of isotopic zoning in lawsonite

5.3.1. Change of syn-metamorphic fluid

In this study, we confirmed, in our knowledge for the first time, isotopic zonation in lawsonites (sample HJK, Fig. 10). The lawsonite in the sample HJK formed at the depth from sub-forearc to sub-arc depth and returned back to the surface possibly along the subduction zone channel

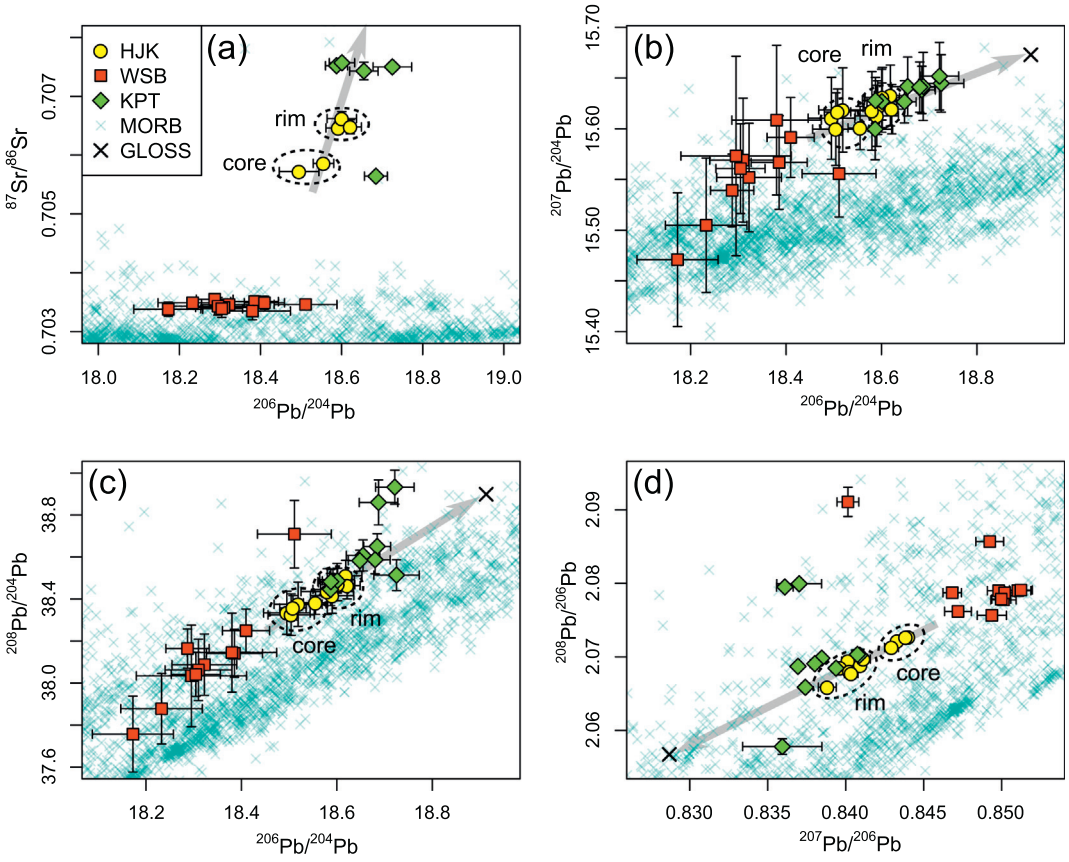

Fig. 10. Enlarged binary plots showing Sr-Pb isotopes of lawsonites. For comparison, MORB (downloaded from the PetDB Database (http://www.earthchem.org/petdb) on 3 July 2018, using following parameter: tectonic setting = SPREADING_CENTER) and sediment (GLOSS; Plank and Langmuir (1998)) are also shown. (a) $^{206}Pb/^{204}Pb$ versus $^{87}Sr/^{86}Sr$ diagram. (b) $^{206}Pb/^{204}Pb$ versus $^{207}Pb/^{204}Pb$ diagram. (c) $^{206}Pb/^{204}Pb$ versus $^{208}Pb/^{204}Pb$ diagram. (d) $^{207}Pb/^{206}Pb$ versus $^{208}Pb/^{206}Pb$ diagram. Gray arrows represent directions toward sedimentary component.

(Tsujimori et al. 2006b). According to Tsujimori et al. (2006b), the sample HJK belongs to Type-II eclogite of the SMM and preserves the second stage eclogite-facies recrystallization (retrograde eclogite stage) with deformation. Considering the lithological information, the isotope modification might have occurred during the second stage. The stage postdates the thermal maximum; the Type-II eclogite might records metamorphism in a mélange of the slab–mantle interface rather than that in the subducted oceanic crust. Therefore, isotopic zoning in the lawsonites is explained by a change in isotopic composition of the source material during its rim overgrowth stage. Since lawsonite-formation requires water, the isotopically different source material would be a water-rich fluid. Considering a significant gap between the cores and the rims (Figs. 7, 8), the newly-delivered synmetamorphic fluid would be external, i.e., infiltrated fluid from the outside of the basaltic protolith. Notably, the rim isotope ratios strongly suggest sediment-derived fluids origin (Fig. 10). The strongly elevated Pb in the bulk-rock composition also supports fluid addition of the sedimentary component. Conclusively, infiltration of such external fluids from a (nearby) metasedimentary rock to the sample HJK metabasaltic rock is the most plausible scenario.

5.3.2. How did the external fluid hydrate the metabasaltic rocks?

Considering a steady-state oceanic subduction, a subducting plate would keep an ocean plate stratigraphy. If a metabasaltic rock occupies stratigraphically upper portion of the subducting plate, the fluids externally infiltrated into the metabasaltic rock likely come from the underlying layer of gabbroic and/or ultramafic rocks (e.g., Hacker et al. 2003). Reaction-induced porosity change would be another possibility of fluid transportation (e.g., Malvoisin 2015). In any case, the slab peridotite beneath the oceanic Moho is characterized by low trace element abundances and MORB-like isotopic compositions (e.g., Workman and Hart 2005) unless a strong seawater alteration took place in the peridotite before subduction. Even so, Pb isotope ratios in the peridotite are unaffected due to low Pb content in the seawater (~1 pg/g in deep seawater, Frank 2002). This solely contradicts a possibility that the isotopic composition of lawsonite rims originated from fluids from the mantle section of the oceanic plate (slab). In a mélange formed at the slab–mantle interface, any metamorphic blocks from different protoliths can suffer extensive external fluid infiltrations from the serpentinized matrix and the underlying oceanic crust. Considering the Sr-Pb isotope compositions of the lawsonite together with trace element patterns (Figs. 6a, b and 10), we interpret that the fluids with a sediment-like isotopic composition, that modified the isotopic composition of the sample HJK, might have infiltrated into the metabasaltic protolith during the post-peak eclogite-facies recrystallization in SMM mélange (retrograde eclogite stage, Tsujimori et al. 2006b). Moreover, the bulk-rock REE pattern of the sample HJK (Fig. 4a) also indicates that the fluid possibly derived from LREE-rich materials such as terrigenous sediments. The bulk-rock LREE abundances of the sample HJK are higher than those of MORB, whereas HREEs are as low as those in MORBs suggesting addition of LREE-rich (sediment) fluids. In summary, LREE-rich and Sr and Pb-rich fluids with radiogenic Sr and Pb infiltrated to form the bulk rock composition of the sample HJK and radiogenic Sr-Pb lawsonite rims.

5.4. Lawsonitology—lawsonite as a new powerful tracer

We stated in Introduction that lawsonite can be used as a proxy of Sr and Pb in the bulk subducted slab materials, especially in the crustal lithologies. Elemental mass balance in this study confirmed the above proposal. Since plate subduction introduces variable oceanic and

continental crust materials into the mantle, the sources of the slab Sr and Pb are also variable. Marschall and Schumacher (2012) proposed a model of high-pressure melting of a mélange. The model suggests that a mélange formed at the slab–mantle interface undergoes fluid-induced partial melting during diapiric upwelling and consequently controls the geochemical signatures of arc magmas. Even if mélange material is not immediately transferred to the mantle depth via diapir, slab fluid flux released from the slab or the mélange interface should be reflected to element mass balance in the arc magmas (Kimura 2017; Kimura et al. 2014). The Sr-Pb isotopic and trace elemental behaviors recorded in the lawsonite crystals in the mélange revealed here will also be reflected to and found in the chemistries of arc magmas.

What is the fate of lawsonite in deeply subducted slab? After decomposition of lawsonite in subducting slab, the remaining trace elements inherited from the precursor lawsonite in some ultra-deep phases may return to the Earth's interior and cycles back to the surface via mantle plumes. The lawsonite in metabasaltic rocks not always preserves its original isotopic compositions in the protolith as shown by this study. But rather the isotopic composition is modified by fluid-mediated metasomatism the most probably in the slab–mantle interface (or mantle wedge) than along with the seawater alteration. Consequently, the isotopic composition either of the sediment layer or of the igneous layer of the subducted slab are strongly modified by the *syn*-metamorphic fluids. This would be a pitfall for discussing isotope trend, heterogeneity, and isotopic growth of the slab residues in the mantle recycling processes (Kimura et al. 2016).

This study utilized the spot analyses of trace element and Sr-Pb isotope ratios of metamorphic lawsonite and successfully obtained geochemical information from these isotopes. Recently, *in-situ* Sr isotope analyses on epidote were performed for Dabieshan ultrahigh-pressure (UHP) eclogites by Guo et al. (2014, 2016). They reported that epidote in amphibolite-facies veinlets has different isotope ratios from the eclogite-stage epidote. They argued multiple source fluid infiltrations during an exhumation of the UHP slab. By contrast, this study revealed the isotopic variations among different lithologies (protoliths) and also revealed the isotope characteristics of syn-metamorphic fluids infiltrated into the lawsonite eclogites by isotopic zoning of lawsonite. Although isotopic zoning of metamorphic minerals has been overlooked among petrologists who tended to assume a chemically close system during metamorphism, our observations urge a more careful assessment of semi-open system metamorphic recrystallization at subduction zone environment. In other words, *in-situ* isotope geochemistry is necessary to discuss complicated geological process.

Our study reconfirmed significance of lawsonite. Considering subduction zone geothermal structure that determines the mineral property, we can emphasize the advantage of lawsonite to decipher behaviors of syn-metamorphic fluids in fossil cold subduction zone complexes. The LA-MC-ICPMS methods used here are powerful tools to obtain considerable amount of isotopic records during short periods of time with reasonable precisions and spatial resolution in 100–200 μm diameter which allows comparisons of the isotopic data with the textural observations. Reconnaissance of *in-situ* isotope analyses for high-pressure metamorphic minerals has just begun. This method will bring new era for the studies of metamorphic rocks, and ultimately contribute to understandings of the subduction zone and the global scale plate tectonic cycles.

6. Conclusions

This study applied *in-situ* spot analyses of Sr-Pb isotope ratios of eclogite-facies metamorphic lawsonites and successfully obtained geochemical information from these isotopes. Sr-Pb isotope compositions revealed compositional variations of the lawsonites reflecting their protoliths and contributions of external fluids derived from different protoliths infiltrated into the late stage lawsonite growth. Considering geological and mineralogical contexts, it is emphasized that lawsonite is the ideal mineral to decipher the behaviors of syn-metamorphic fluids in paleo subduction zones. LA-MC-ICPMS method can provide plenty of isotope data in a short term with reasonable precisions and spatial resolutions usable for comparisons with the observed metamorphic textures. This powerful method will greatly promote the studies of metamorphic rocks.

Acknowledgement

This research was supported by Center for Northeast Asian Studies, Tohoku University and the Japan Agency for Marine-Earth Science and Technology (JAMSTEC) in part by grants from the MEXT/JSPS KAKENHI (JP15H05212 and JP18H01299) to T. Tsujimori and KAKENHI (JP15H02148, JP16H01123, and JP18H04372) to J.-I. Kimura. We are grateful for constructive reviews from Alberto Vitale-Brovarone and an anonymous reviewer. This manuscript was also improved by Daniel Pastor-Galán. We thank K. Flores and G.E. Harlow for providing the latest version of the geological map of the Motagua Mélange.

Appendix A. Supplementary data

Supplementary data to this article can be found online at https://doi.org/10.1016/j.lithos.2018.09.001.

References

Brueckner, H.K., Avé Lallemant, H.G., Sisson, V.B., Harlow, G.E., Hemming, S.R., Martens, U., Tsujimori, T., Sorensen, S.S., 2009. Metamorphic reworking of a high pressure–low temperature mélange along the Motagua fault, Guatemala: a record of Neocomian and Maastrichtian transpressional tectonics. Earth Planet. Sci. Lett. 284, 228–235.

Clarke, G.L., Powell, R., Fitzherbert, J.A., 2006. The lawsonite paradox: a comparison of field evidence and mineral equilibria modelling. J. Metamorph. Geol. 24, 715–725.

Flores, K.E., Martens, U.C., Harlow, G.E., Brueckner, H.K., Pearson, N.J., 2013. Jadeitite formed during subduction: in situ zircon geochronology constraints from two different tectonic events within the Guatemala Suture Zone. Earth Planet. Sci. Lett. 371, 67–81.

Frank, M., 2002. Radiogenic isotopes: tracers of past ocean circulation and erosional input. Rev. Geophys. 40, 1–38.

Guo, S., Ye, K., Yang, Y., Chen, Y., Zhang, L., Liu, J., Mao, Q., Ma, Y., 2014. In situ Sr isotopic analyses of epidote: tracing the sources of multistage fluids in ultrahigh-pressure eclogite, Ganghe, Dabie terrane. Contrib. Mineral. Petrol. 167, 975.

Guo, S., Yang, Y., Chen, Y., Su, B., Gao, Y., Zhang, L., Liu, J., Mao, Q., 2016. Grain-scale Sr isotope heterogeneity in amphibolite, retrograded UHP eclogite, Dabie terrane: Implications for the origin and flow behavior of retrograde fluids during slab exhumation. Lithos 266, 383–405.

Hacker, B.R., Abers, G.A., Peacock, S.M., 2003. Subduction factory 1. Theoretical mineralogy, densities, seismic wave speeds, and H_2O contents. J. Geophys. Res. Solid Earth 108.

Harlow, G.E., Hemming, S.R., Lallemant, H.G.A., Sisson, V.B., Sorensen, S.S., 2004. Two high-pressure–low-temperature serpentinite-matrix mélange belts, Motagua fault zone, Guatemala: a record of Aptian and Maastrichtian collisions. Geology 32, 17–20.

Harlow, G.E., Flores, K.E., Marschall, H.R., 2016. Fluid-mediated mass transfer from a paleosubduction channel to its mantle wedge: evidence from jadeitite and related rocks from the Guatemala Suture Zone. Lithos 258, 15–36.

Hermann, J., 2002. Allanite: thorium and light rare earth element carrier in subducted crust. Chem. Geol. 192, 289–306.

Hirahara, Y., Kimura, J.-I., Senda, R., Miyazaki, T., Kawabata, H., Takahashi, T., Chang, Q., Vaglarov, B.S., Sato, T., Kodaira, S., 2015. Geochemical variations in Japan Sea back-arc basin basalts formed by high-temperature adiabatic melting of mantle metasomatized by sediment subduction components. Geochem. Geophys. Geosyst. 16, 1324–1347.

Jaffey, A., Flynn, K., Glendenin, L., Bentley, W.T., Essling, A., 1971. Precision measurement of half-lives and specific activities of ^{235}U and ^{238}U. Phys. Rev. C 4, 1889.

Kessel, R., Schmidt, M.W., Ulmer, P., Pettke, T., 2005. Trace element signature of subduction-zone fluids, melts and supercritical liquids at 120–180 km depth. Nature 437, 724.

Kimura, J.-I., 2017. Modeling chemical geodynamics of subduction zones using the Arc Basalt Simulator version 5. Geosphere 13, 992–1025.

Kimura, J.-I., Chang, Q., 2012. Origin of the suppressed matrix effect for improved analytical performance in determination of major and trace elements in anhydrous silicate samples using 200 nm femtosecond laser ablation sectorfield inductively coupled plasma mass spectrometry. J. Anal. At. Spectrom. 27, 1549–1559.

Kimura, J.-I., Kawabata, H., Chang, Q., Miyazaki, T., Hanyu, T., 2013a. Pb isotope analyses of silicate rocks and minerals with Faraday detectors using enhanced-sensitivity laser ablation-multiple collector-inductively coupled plasma mass spectrometry. Geochem. J. 47, 369–384.

Kimura, J.-I., Takahashi, T., Chang, Q., 2013b. A new analytical bias correction for in situ Sr isotope analysis of plagioclase crystals using laser-ablation multiple-collector inductively coupled plasma mass spectrometry. J. Anal. At. Spectrom. 28, 945–957.
Kimura, J.-I., Gill, J.B., Kunikiyo, T., Osaka, I., Shimoshioiri, Y., Katakuse, M., Kakubuchi, S., Nagao, T., Furuyama, K., Kamei, A., et al., 2014. Diverse magmatic effects of subducting a hot slab in SW Japan: results from forward modeling. Geochem. Geophys. Geosyst. 15, 691–739.
Kimura, J.-I., Gill, J.B., Skora, S., van Keken, P.E., Kawabata, H., 2016. Origin of geochemical mantle components: Role of subduction filter. Geochem. Geophys. Geosyst. 17, 3289–3325.
Klimm, K., Blundy, J.D., Green, T.H., 2008. Trace element partitioning and accessory phase saturation during H_2O-saturated melting of basalt with implications for subduction zone chemical fluxes. J. Petrol. 49, 523–553.
Li, J.-L., Gao, J., John, T., Klemd, R., Su, W., 2013. Fluid-mediated metal transport in subduction zones and its link to arc-related giant ore deposits: constraints from a sulfide-bearing HP vein in lawsonite eclogite, Tianshan, China. Geochim. Cosmochim. Acta 120, 326–362.
Malvoisin, B., 2015. Mass transfer in the oceanic lithosphere: serpentinization is not isochemical. Earth Planet. Sci. Lett. 430, 75–85.
Marschall, H.R., Schumacher, J.C., 2012. Arc magmas sourced from mélange diapirs in subduction zones. Nat. Geosci. 5, 862–867.
Martin, L., Hermann, J., Gauthiez-Putallaz, L., Whitney, D., Vitale Brovarone, A., Fornash, K., Evans, N.J., 2014. Lawsonite geochemistry and stability– implication for trace element and water cycles in subduction zones. J. Metamorph. Geol. 32, 455–478.
McDonough, W.F., Sun, S.-S., 1995. The composition of the Earth. Chem. Geol. 120, 223–253.
Mulcahy, S.R., King, R.L., Vervoort, J.D., 2009. Lawsonite Lu-Hf geochronology: a new geochronometer for subduction zone processes. Geology 37, 987–990.
Okamoto, K., Maruyama, S., 1999. The high-pressure synthesis of lawsonite in the MORB + H_2O system. Am. Mineral. 84, 362–373.
Pawley, A.R., Redfern, S.A., Holland, T.J.B., 1996. Volume behavior of hydrous minerals at high pressure and temperature: I. Thermal expansion of lawsonite, zoisite, clinozoisite, and diaspore.
Pearce, J.A., Harris, N.B., Tindle, A.G., 1984. Trace element discrimination diagrams for the tectonic interpretation of granitic rocks. J. Petrol. 25, 956–983.
Plank, T., Langmuir, C.H., 1998. The chemical composition of subducting sediment and its consequences for the crust and mantle. Chem. Geol. 145, 325–394.
Pouchou, J., Pichoir, F., Boivin, D., 1990. The XPP Procedure Applied to Quantitative EDS X-Ray Analysis in the SEM. Microbeam Analysis, pp. 120–126.
Ringwood, A.E., 1974. The petrological evolution of island arc systems: Twenty-seventh William Smith Lecture. J. Geol. Soc. 130, 183–204.
Ringwood, A.E., 1991. Phase transformations and their bearing on the constitution and dynamics of the mantle. Geochim. Cosmochim. Acta 55, 2083–2110.
Rosman, K., Taylor, P., 1998. Isotopic compositions of the elements 1997, technical report. Pure Appl. Chem. 70, 217–235.
Schmidt, M.W., Poli, S., 1998. Experimentally based water budgets for dehydrating slabs and consequences for arc magma generation. Earth Planet. Sci. Lett. 163, 361–379.
Spandler, C., Hermann, J., Arculus, R., Mavrogenes, J., 2003. Redistribution of trace elements during prograde metamorphism from lawsonite blueschist to eclogite facies; implications for deep subduction-zone processes. Contrib. Mineral. Petrol. 146, 205–222.
Stalder, R., Foley, S.F., Brey, G.P., Horn, I., 1998. Mineral-aqueous fluid partitioning of trace elements at 900–1200 °C and 3.0–5.7 GPa: New experimental data for garnet, clinopyroxene, and rutile, and implications for mantle metasomatism. Geochim. Cosmochim. Acta 62, 1781–1801.
Sun, S.S., McDonough, W.S., 1989. Chemical and isotopic systematics of oceanic basalts: implications for mantle composition and processes. Geol. Soc. Lond., Spec. Publ. 42, 313–345.
Tatsumi, Y., Sakuyama, M., Fukuyama, H., Kushiro, I., 1983. Generation of arc basalt magmas and thermal structure of the mantle wedge in subduction zones. J. Geophys. Res. Solid Earth 88, 5815–5825.
Tribuzio, R., Messiga, B., Vannucci, R., Bottazzi, P., 1996. Rare earth element redistribution during high-pressure–low-temperature metamorphism in ophiolitic Fe-gabbros, Liguria, northwestern Italy: Implications for light REE mobility in subduction zones. Geology 24, 711–714.
Tsujimori, T., Ernst, W., 2014. Lawsonite blueschists and lawsonite eclogites as proxies for palaeo-subduction zone processes: a review. J. Metamorph. Geol. 32, 437–454.
Tsujimori, T., Liou, J.G., Coleman, R.G., 2005. Coexisting retrograde jadeite and omphacite in a jadeite-bearing lawsonite eclogite from the Motagua Fault Zone. Guatemala. Am. Mineral. 90, 836–842.
Tsujimori, T., Sisson, V.B., Liou, J.G., Harlow, G.E., Sorensen, S.S., 2006a. Very-low-temperature record of the subduction process: a review of worldwide lawsonite eclogites. Lithos 92, 609–624.
Tsujimori, T., Sisson, V.B., Liou, J.G., Harlow, G.E., Sorensen, S.S., 2006b. Petrologic Characterization of Guatemalan Lawsonite Eclogite: Eclogitization of Subducted Oceanic Crust in a Cold Subduction Zone. Vol. 403. Geological Society of America Special Papers, pp. 147–168.
Ueno, T., 1999. REE-bearing sector-zoned lawsonite in the Sanbagawa pelitic schists of the eastern Kii Peninsula, Central Japan. Eur. J. Mineral. 11, 993–998.
Veizer, J., Ala, D., Azmy, K., Bruckschen, P., Buhl, D., Bruhn, F., Carden, G.A., Diener, A., Ebneth, S., Godderis, Y., et al., 1999. $^{87}Sr/^{86}Sr$, $\delta^{13}C$ and $\delta^{18}O$ evolution of Phanerozoic seawater. Chem. Geol. 161, 59–88.
Vitale Brovarone, A., Beyssac, O., 2014. Lawsonite metasomatism: a new route for water to the deep Earth. Earth Planet. Sci. Lett. 393, 275–284.
Vitale Brovarone, A., Alard, O., Beyssac, O., Martin, L., Picatto, M., 2014. Lawsonite metasomatism and trace element recycling in subduction zones. J. Metamorph. Geol. 32, 489–514.
White, W.M., 1985. Sources of oceanic basalts: radiogenic isotopic evidence. Geology 13, 115–118.
Whitney, D.L., Davis, P.B., 2006. Why is lawsonite eclogite so rare? Metamorphism and preservation of lawsonite eclogite, Sivrihisar, Turkey. Geology 34, 473–476.
Whitney, D.L., Evans, B.W., 2010. Abbreviations for names of rock-forming minerals. Am. Mineral. 95, 185–187.
Workman, R.K., Hart, S.R., 2005. Major and trace element composition of the depleted MORB mantle, DMM. Earth Planet. Sci. Lett. 231, 53–72.
Zindler, A., Hart, S.R., 1986. Chemical geodynamics. Annu. Rev. Earth Planet. Sci. 14, 493–571.